International Journal of Engineering

Super-resolution of Defocus Blurred Images

S. J. Seyyedyazdi, H. Hassanpour*

Image Processing and Data Mining (IPDM) Research Lab, Faculty of Computer Engineering and Information Technology, Shahrood University of Technology, Shahrood, Iran

P A P E R   I N F O

A B S T R A C T

Super-resolution is a process that combines information from some low-resolution images in order to produce an image with higher resolution. In most of the previous related work, the blurriness that is associated with low resolution images is assumed to be due to the integral effect of the acquisition device's image sensor. However, in practice there are other sources of blurriness as well, including atmospheric and motion blur that may be applied to low resolution images. The research done in this paper provides a super-resolution image from some low-resolution images suffering from blurriness due to defocus. In contrast to motion blur kernels that are sparse, the defocus blur kernel is non-sparse and continuous. Because of the continuity property of defocus blurring kernel, in this paper, we bound the gradient of blurring kernel using proper regularizers to satisfy this property. Experimental results on synthetic data demonstrate the effectiveness of the proposed method to produce high resolution and de-blurred images from some blurry low-resolution images.

1. INTRODUCTION

Multi input super-resolution (SR) technique makes a high resolution (HR) image by combining some low resolution (LR) images from the same scene. The LR images are similar, but not identical. To produce such LR images the acquisition device is moved and/or rotated slightly each time a LR image is taken. These movements, known as warping, due to the sampling resolution limitation of the imaging sensor, cause each LR image to have different information. The SR combines this information to produce a HR image.

SR is an inverse problem, meaning that it reverses the process of making LR images. LR images are made according to (1), known as observation or degradation model.

$$\mathbf{y}_k = \mathbf{D} \times \mathbf{W}_k \times \mathbf{H}_k \times \mathbf{x} + \mathbf{n}, \ k = 1, \dots, L \qquad (1)$$

where, $\mathbf{x}$ is an $NP \times 1$ vector representing HR image and $\mathbf{y}_k$ $N \times 1$ k-th LR image vector, both are lexicographically represented and P is the factor of increase in resolution. $\mathbf{D}$ is $N \times NP$ down-sampling matrix, $\mathbf{W}_k$ and $\mathbf{H}_k$ are $NP \times NP$ matrices representing

the warping and blurring operators, respectively, and $\mathbf{n}$, an $N \times 1$ vector, models all noise of the process. According to observation model (1), HR image $\mathbf{x}$, (i.e. the ideal image of the scene), is blurred, warped and down-sampled, then contaminated by some noise to generate an LR image. The blurring operator $\mathbf{H}_k$ is obtained from $\mathbf{h}_k$, the blur kernel that is applied on kth LR image.

To align all LR images, one of them, say $\mathbf{y}_r$, is chosen as a reference LR image. The alignment is performed by an image registration algorithm as a step in SR process or pre-computed beforehand.

In most of the recent works (e.g. [1]), the blurriness to the LR images is known and is assumed to be due to the integral property of imaging sensor. However in practice, there are some other sources of blurring, such as out-of-focus blur, atmospheric blur and motion blur and often the blurriness is unknown. In previous work, we proposed a method to estimate the blur kernel associated with the HR image, using the LR image blurriness [2]. In this paper, we assume that the applied blur is due to out-of-focus with unknown parameter and is the same for all the LR images (i.e. $\mathbf{h}_k = \mathbf{h}, \ k = 1, \dots, L$). This

---

Corresponding Author Email: h.hassanpour@shahroodut.ac.ir (H. Hassanpour)

assumption is fair, since the settings of acquisition process is identical for all the LR images taken from a scene in a short period of time.

One problem in reconstructing $\mathbf{x}$ given $\mathbf{y}$ is the boundary pixels and the pixels near them. These pixels, due to blurring effect, depend on pixels located outside the boundary. To address this issue, one can make some assumptions about the pixels that are outside $\mathbf{y}$, known as boundary condition (BC). While there are some boundary conditions such as periodic BC and zero BC that are commonly adopted by the researchers, none of them is accurate in practice. Similar to the work in [3], we exclude the boundary of the reconstructed image, by applying a masking matrix $\mathbf{M} \in \{0,1\}^{n \times m}$. Hence, taking into account the identical blur kernel for each LR and applying the masking matrix, the observation model in this paper can be represented as:

$$\mathbf{y}_k = \mathbf{DW}_k\mathbf{MHx} + \mathbf{n}, \ k = 1, \dots, L. \tag{2}$$

In (2), $\mathbf{Hx}$ is corresponding to a same shape convolution (i.e. the size of $\mathbf{Hx}$ is the same as $\mathbf{x}$) and $\mathbf{MHx}$ is corresponding to a valid shape convolution.

Organization of this paper is as follows. In Section 2, we briefly review some previous related researches. Our method is proposed in Section 3. In Section 4 experimental results are reported and finally, Section 5 concludes the paper.

2. BACKGROUND

Super-resolution was initially developed by Tsai and Huang in 1970s [4]. They formulated the problem in frequency domain and used the shifting property of Fourier Transform to reconstruct HR image. The frequency domain approach for SR problem assumes that the warping applied to LR images is pure translation, i.e. no rotation is allowed. This assumption is a major limitation and a considerable deficiency in obtaining the SR image. Hence, development of SR algorithms was switched to spatial domain by the researchers.

Observation model is a key factor in developing the SR algorithm. There are two main observation models: blur-warp and warp-blur [5]. In blur-warp model, as in (1), the ideal image $\mathbf{x}$ is first blurred and then warped. Some authors use this model (eg. [6]). In contrast, in warp-blur model, the warping of $\mathbf{x}$ is applied before blurring. The difference of these models is discussed in [7]. Using blur-warp model, the blur HR image can be straightforwardly estimated using optimization technique. Thus the SR problem is converted to a Blind Image Deconvolution (BID) problem. This approach, which has been used in some researches (e.g. [6], [8], and [9]), is employed in this paper. More details are provided in the next section.

Algorithm 1. HR Blur Image estimation

1	initialize $\mathbf{b}$, choose γ and thr.
2	**while** true
3	$\quad \nabla_\mathbf{b} \leftarrow \sum_{k=1}^{L} -2(\mathbf{DW}_k)^T(\mathbf{y}_k - \mathbf{DW}_k\mathbf{b})$
4	$\quad \mathbf{b}_{new} \leftarrow \mathbf{b} - \gamma\nabla_\mathbf{b}$
5	$\quad$ If $(\|\mathbf{b}_{new} - \mathbf{b}\| < thr)$ break
6	$\quad b \leftarrow \mathbf{b}_{new}$
7	**end while**

SR and BID are both inverse and ill-posed problems. Meaning that, given blur image $\mathbf{b}$, there are many pairs of image $\mathbf{x}$ and blur kernel $\mathbf{h}$ that $\mathbf{b}$ can be produced by convolving them. (e.g. $\mathbf{x} = \mathbf{b}$ and $\mathbf{h}$: identity filter). So, additional information about unknowns must be provided to obtain a useful solution. This information can be supplied by regularization. Studies have shown that the gradients of natural images is sparse and have a heavy-tailed distribution [10, 11]. Hence, we use the hyper-Laplacian distribution that is a way to model heavy-tailed distribution and is frequently used in literature (e.g., [12]), as a proper regularizer for latent image.

As latent HR image, unknown blur kernel needs regularizer too. Almeida and Figueiredo in [13] used positivity constraint for blur kernel (i.e. entries of blur kernel must be positive). In contrast to motion blur kernels that typically are sparse, defocus blur kernels are non-sparse and continuous. To achieve this non-sparsity, in addition to positivity constraint, we introduce a new regularizer to limit the gradient of the blur kernel. The details are addressed in the next section.

3. PROPOSED METHOD

Similar to some previous researches (e.g. [8] and [6]), our proposed SR process comprises of two phases. In the first step, the blurred high resolution image, $\mathbf{b} = \mathbf{MHx}$, is recovered. Then, in the second step, $\mathbf{b}$ is de-blurred to produce $\mathbf{x}$. To recover the blurred HR image, $\mathbf{b}$, we use gradient descend (GD) algorithm. Then, to reconstruct the HR image, $\mathbf{x}$, and blur kernel, $\mathbf{h}$, we use an iterative alternating optimization approach using Alternating Direction Method of Multipliers (ADMM) [14].

Super-resolution and de-blurring are both ill-posed inverse problems. To solve such problems, we need some additional information about the solution, known as regularizations. In this research, we use gradient of image as well as gradient of blur kernel as regularizers. The following subsections clarify our proposed method.

3. 1. Estimating HR Blur Image
Based on the observation model (2), the HR blur image $\mathbf{b} = \mathbf{MHx}$ is the solution of the optimization Equation (3):

$$\hat{\mathbf{b}} = \arg\min_b \sum_{k=1}^{L} \|\mathbf{y}_k - \mathbf{DW}_k\mathbf{b}\|_2^2 \tag{3}$$

To solve (3), we simply use the gradient descent (GD)

method [15] illustrated in Algorithm 1. In this algorithm, **b** is initialized by the up-sampled version of the reference LR image.

Algorithm 2. Blind Image Deconvolution

1	set $\hat{\mathbf{h}}$ to identity filter and $\boldsymbol{\lambda} = \boldsymbol{\lambda}_0$;
2	**repeat**
3	$\quad \hat{\mathbf{x}} \leftarrow \arg\min_{\mathbf{x}} J_\lambda(\mathbf{x}, \hat{\mathbf{h}})$
4	$\quad \hat{\mathbf{h}} \leftarrow \arg\min_{\mathbf{h}} J_\lambda(\hat{\mathbf{x}}, \mathbf{h})$
5	$\quad$ update λ
6	**until** stopping criteria is satisfied

3. 2. Blind Image Deconvolution

After estimating **b**, the SR problem reduces to BID, that is, estimating latent HR image **x** as well as the unknown blur kernel **h**. These unknowns can be estimated alternatively: first, by initializing the blur kernel as identity filter, the latent image **x** is estimated; then, given the estimated latent image, the blur kernel is estimated. This process is repeated until some criteria are satisfied. The details are illustrated inAlgorithm 2, where $J_\lambda(\mathbf{x}, \mathbf{h})$ is the cost function and λ is the regularization parameters that will be introduced later.

In most deblurring methods, FFT-based convolution is used assuming periodic boundary condition (e.g. [12]). However, in practice the boundary condition is unknown. To take into account the unknown boundary conditions, as [3] we exclude the boundary of desired HR image using a masking matrix. Hence, our problem is formulated as a combination of blind image deconvolution and inpainting problem.

As mentioned earlier, BID is an inverse and ill-posed problem. Hence, appropriate regulizers must be used to obtain useful solutions. Therefore, the following cost function is used in this paper to estimate the latent HR image and the blur kernel.

$$J_\lambda(\mathbf{x}, \mathbf{h}) = \left\| \hat{\mathbf{b}} - \mathbf{MHx} \right\|_2^2 + \lambda_1 R_1(\mathbf{x}) + \lambda_2 R_2(\mathbf{x}) + \lambda_h R_h(\mathbf{h}) \tag{4}$$

where, the first term is data-fidelity that penalizes inconsistency between the latent HR image **x** and the blur HR image $\hat{\mathbf{b}}$; $R_1(\mathbf{x})$, $R_2(\mathbf{x})$ and $R_h(\mathbf{h})$ are regularization functions that are defined later, and λ_1, λ_2 and λ_h are the corresponding regularization parameters. In Algorithm 2, $\boldsymbol{\lambda}$ is defined as $\boldsymbol{\lambda} = [\lambda_1, \lambda_2, \lambda_h]$. As mentioned earlier, $\mathbf{M} \in \{0,1\}^{n \times m}$ is a masking matrix that excludes the boundary pixels of the image. Similar to [9], in this paper we use generalized total variation (GTV) regularizer as $R_1(\mathbf{x})$ which is defined as (5):

$$R_1(\mathbf{x}) = \|\mathbf{D}_0\mathbf{x}\|_q^q + \|\mathbf{D}_{45}\mathbf{x}\|_q^q + \|\mathbf{D}_{90}\mathbf{x}\|_q^q + \|\mathbf{D}_{135}\mathbf{x}\|_q^q \tag{5}$$

where, $\mathbf{D}_\theta, \theta \in \{0, 45, 90, 135\}$ is a partial derivative operator in direction that makes a θ degree angle with positive x-axis. As mentioned earlier, distribution of gradients of natural images can be modeled by hyper-

Laplacian distribution [12], this can be done by setting $q \in (0, 1)$.

Algorithm 3. Scaled ADMM

1	Set $k = 0$, choose $\mu^{(j)} > 0$, $\mathbf{u}_0^{(j)}$, and $\mathbf{d}_0^{(j)}$, for $j = 1, \dots, J$.
2	**Repeat**
3	$\quad \mathbf{r}_{k+1} \leftarrow \sum_{j=1}^J \mu^{(j)} \left(\mathbf{G}^{(j)}\right)^T \left(\mathbf{u}_k^{(j)} + \mathbf{d}_k^{(j)}\right)$
4	$\quad \mathbf{z}_{k+1} \leftarrow \left[\sum_{j=1}^J \mu^{(j)} \left(\mathbf{G}^{(j)}\right)^T \mathbf{G}^{(j)}\right]^{-1} \mathbf{r}_{k+1}$
5	$\quad$ **for** $j = 1 \ to \ J$ **do**
6	$\quad\quad \mathbf{u}_{k+1}^{(j)} \leftarrow \text{prox}_{g^{(j)}/\mu^{(j)}} \left(\mathbf{G}^{(j)}\mathbf{z}_{k+1} - \mathbf{d}_k^{(j)}\right)$
7	$\quad\quad \mathbf{d}_{k+1}^{(j)} \leftarrow \mathbf{d}_k^{(j)} - \left(\mathbf{G}^{(j)}\mathbf{z}_{k+1} - \mathbf{u}_k^{(j)}\right)$
8	$\quad$ **End**
9	$\quad k \leftarrow k + 1$
10	**until** stopping criteria is satisfied

Experiments in [16] show that the second-order gradients of natural images have also heavy-tailed distribution. Hence, we use the regularizer (6) as $R_2(\mathbf{x})$:

$$R_2(\mathbf{x}) = \|\mathbf{D}_{xx}\mathbf{x}\|_q^q + \|\mathbf{D}_{xy}\mathbf{x}\|_q^q + \|\mathbf{D}_{yy}\mathbf{x}\|_q^q \tag{6}$$

where, $\mathbf{D}_{xx}$, $\mathbf{D}_{xy}$ and $\mathbf{D}_{yy}$ are second-order derivative operators in horizontal, vertical and diagonal direction, respectively.

As mentioned earlier, the focus of this paper is on super-resolution of out-of-focus blur LR images. In contrast to motion blur kernel that is typically sparse, out-of-focus blur kernel can be modeled as a disk kernel and is continuous. To force blur kernel to be continuous, we set $R_h(\mathbf{h})$ as (7).

$$R_h(\mathbf{h}) = \|\mathbf{D}_{45}\mathbf{h}\|_1 + \|\mathbf{D}_{135}\mathbf{h}\|_1 \tag{7}$$

The regulizer (7) limits the gradient of the kernel in two orthogonal directions. These directions are found experimentally.

3. 3. ADMM Algorithm

To solve the cost function in (4), we use the Alternating Direction Method of Multipliers (ADMM) algorithm [14]. The ADMM algorithm is suitable to solve the following unconstrained minimization problem:

$$\min_{\mathbf{z} \in \mathbb{R}^d} \sum_{j=1}^J g^{(j)}(\mathbf{G}^{(j)}\mathbf{z}) \tag{8}$$

where, $G^{(g)} \in \mathbb{R}^{p_j \times d}$ are arbitrary matrices and $g^{(j)}: \mathbb{R}^{p_j} \to \mathbb{R}$ are functions. Equation (8) can be rewriten as the constrained minimization (9), where $\mathbf{u}^{(j)}$ is the splitting variable.

$$\min_{\mathbf{z} \in \mathbb{R}^n, \mathbf{u}^{(1)} \in \mathbb{R}^{p_1}, \dots, \mathbf{u}^{(J)} \in \mathbb{R}^{p_J}} \sum_{j=1}^J g^{(j)}\left(\mathbf{u}^{(j)}\right) \tag{9}$$

subject to $\mathbf{u}^{(j)} = \mathbf{G}^{(j)}\mathbf{z}$, for $j = 1, \dots, J$.

The ADMM algorithm to solve (9) is presented in Algorithm 3 where, the $\mathbf{d}^{(j)}$ is a dual variable and $\mu^{(j)}$ is ADMM's penalty parameter. In line 6 of the algorithm,

$\mathrm{prox}_{g^{(j)}/\mu^{(j)}}$ is the proximity operator of $g^{(j)}/\mu^{(j)}$. Proximity operator of function f is defined as:
$\mathrm{prox}_f(\mathbf{v}) = \arg\min_{\mathbf{x}}\frac{1}{2}\|\mathbf{v} - \mathbf{x}\|_2^2 + f(\mathbf{x})$.

3. 4. Estimating High Resolution Image

To estimate HR image (line 3 of Algorithm 3), we solve the following minimization problem

$$\hat{\mathbf{x}} = \arg\min_{\mathbf{x}}\left\|\hat{\mathbf{b}} - \mathbf{MHx}\right\|_2^2 + \lambda_1 R_1(\mathbf{x}) + \lambda_2 R_2(\mathbf{x}) \tag{10}$$

To solve (10) using ADMM, the following setting is used: $J = 8$ and

$$\mathbf{G}^{(1)} = \mathbf{H} \tag{11}$$

$$\mathbf{G}^{(2)} = \mathbf{D}_0, \quad \mathbf{G}^{(3)} = \mathbf{D}_{45}, \\ \mathbf{G}^{(4)} = \mathbf{D}_{90}, \quad \mathbf{G}^{(5)} = \mathbf{D}_{135} \tag{12}$$

$$\mathbf{G}^{(6)} = \mathbf{D}_{xx}, \mathbf{G}^{(7)} = \mathbf{D}_{xy}, \mathbf{G}^{(8)} = \mathbf{D}_{yy} \tag{13}$$

$$g^{(1)}\left(\mathbf{u}^{(1)}\right) = \frac{1}{2}\left\|\mathbf{y} - \mathbf{Mu}^{(1)}\right\|_2^2 \tag{14}$$

$$g^{(j)}\left(\mathbf{u}^{(j)}\right) = \lambda_j\left\|\mathbf{u}^{(j)}\right\|_q^q, \quad j = 2, \dots, 8 \tag{15}$$

where,

$$\lambda_j = \begin{cases} \lambda_1 & j = 2, \dots, 5 \\ \lambda_2 & j = 6, 7, 8 \end{cases} \tag{16}$$

In performing Algorithm 3, the main steps are lines 4 and 6. Substituting (11) through (15), line 4 of the algorithm can be written as

$$\mathbf{z}_{k+1} \leftarrow \mathbf{A}\left(\sum_{j=1}^{8}\mu^{(j)}\left(\mathbf{G}^{(j)}\right)^T\left(\mathbf{u}_k^{(j)} + \mathbf{d}_k^{(j)}\right)\right) \tag{17}$$

where,

$$\mu^{(j)} = \begin{cases} \mu_1 & j = 1 \\ \mu_2 & j = 2, \dots, 5 \\ \mu_3 & j = 6, 7, 8 \end{cases} \tag{18}$$

and

$$\mathbf{A} = \left(\sum_{j=1}^{8}\mu^{(j)}\left(\mathbf{G}^{(j)}\right)^T\mathbf{G}^{(j)}\right)^{-1} \tag{19}$$

Solving line 6 of Algorithm 3 leads to the following proximity operators:

$$\mathrm{prox}_{g^{(1)}/\mu_1}(\mathbf{v}) = \arg\min_{\mathbf{x}}\frac{1}{\mu_1}\|\mathbf{y} - \mathbf{Mx}\|_2^2 + \\ \frac{1}{2}\|\mathbf{v} - \mathbf{x}\|_2^2 = (\mu_1\mathbf{I} + \mathbf{M}^T\mathbf{M})^{-1}(\mathbf{M}^T\mathbf{y} + \mu_1\mathbf{v}) \tag{20}$$

$$\mathrm{prox}_{g^{(j)}/\mu^{(j)}}(\mathbf{v}) = \arg\min_{\mathbf{x}}\frac{\lambda_j}{\mu^{(j)}}\|\mathbf{x}\|_q^q + \frac{1}{2}\|\mathbf{v} - \\ \mathbf{x}\|_2^2, j = 1, \dots, 8. \tag{21}$$

where, $\mathbf{I}$ in (20) is an identity matrix and $\mu^{(j)}$ is as (18).

Equation (20) can easily be computed as discussed in [13]. Equation (21) has a closed form solution only for $q \in \{0, \frac{1}{2}, \frac{2}{3}, 1, \frac{4}{3}, \frac{3}{2}, 2\}$. For other values of q, one can

solve the equation numerically and keep the solution in a lookup table for later iterations [12]; the same approach is used in this paper.

3. 5. Estimating Blur Kernel

To estimate the blur kernel $\mathbf{h}$, step 4 in Algorithm 2, the following minimization problem must be solved by another instance of Algorithm 3.

$$\hat{\mathbf{h}} = \arg\min_{\mathbf{x}}\left\|\hat{\mathbf{b}} - \mathbf{MXh}\right\|_2^2 + \lambda_h R_h(\mathbf{h}) , \tag{22}$$

where, $\mathbf{X}$ is convolution matrix corresponding to latent image $\mathbf{x}$, such that $\mathbf{Hx} = \mathbf{Xh}$.

The ADMM settings for solving (22) are: $J = 3$,

$$\mathbf{G}^{(1)} = \mathbf{X} \tag{23}$$

$$\mathbf{G}^{(2)} = \mathbf{D}_{45}, \quad \mathbf{G}^{(3)} = \mathbf{D}_{135} \tag{24}$$

$$g^{(1)}\left(\mathbf{u}^{(1)}\right) = \frac{1}{2}\left\|\mathbf{y} - \mathbf{Mu}^{(1)}\right\|_2^2 \tag{25}$$

$$g^{(j)}\left(\mathbf{u}^{(j)}\right) = \lambda_1\left\|\mathbf{u}^{(j)}\right\|_q^q, \quad j = 2, 3 \tag{26}$$

Substituting the above equations in Algorithm 3 leads to:

$$\mathbf{z}_{k+1} \leftarrow \mathbf{B}\left(\mu^{(1)}\mathbf{X}^T\left(\mathbf{u}_k^{(1)} + \mathbf{d}_k^{(1)}\right) + \\ \mu^{(2)}\mathbf{D}_{45}^T\left(\mathbf{u}_k^{(2)} + \mathbf{d}_k^{(2)}\right) + \mu^{(2)}\mathbf{D}_{135}^T\left(\mathbf{u}_k^{(3)} + \mathbf{d}_k^{(3)}\right)\right), \tag{27}$$

where, $\mathbf{B} = \left(\mu^{(1)}\mathbf{X}^T\mathbf{X} + \mu^{(2)}\sum_{j=2}^3\mathbf{G}_j^T\mathbf{G}_j\right)^{-1}$ and

$$\mu^{(j)} = \begin{cases} \rho_1 & j = 1 \\ \rho_2 & j = 2, 3 \end{cases} \tag{28}$$

Proximity operator of $g^{(1)}/\mu^{(1)}$ is similar to (20) and proximity operator of $g^{(j)}/\mu^{(j)}, j = 2, 3$, is also similar to (21).

Finally, after estimating the blur kernel in (27), its negative entries are set to zero.

4. EXPERIMENTS

To evaluate the proposed method, we apply it on some synthetic LR images. The LR images are produced according to observation model (2) from 10 images depicted in Figure 1 and three blur kernels of size 7×7, 11×11 and 15×15. We set the factor of increase in resolution to 2 ($P = 2$) and SNR about 50.

In the experiments, the parameters are experimentally initialized as follows: $\lambda_1 = 1$, $\lambda_2 = 0.16$, $\lambda_h = 0.1$, $q = 0.8$, $\mu_1 = 1$, $\mu_2 = \lambda_1/2$, $\mu_3 = \lambda_2/2$, $\rho_1 = 1$, $\rho_2 = \lambda_h/2$. Updating λ (line 5 of Algorithm 2) is done as $\lambda_i = \max(\alpha\lambda_i, \epsilon_i), i = 1, 2$, where $\alpha = 0.7$ and $\epsilon_1 = \epsilon_2 = 10^{-6}$ and λ_h is fixed in all iterations.

In our implementation, varying penalty parameters, described in [14], are used to adaptively change all $\mu^{(j)}$

Figure 1. Images used in our first experiments

in each iteration of both instances of ADMM algorithm. Similar to [13], the image estimate (line 3 of Algorithm 2) is computed with 20 iteration of the first instance of Algorithm 3 and initialized with $\mathbf{d}_0^{(j)} = 0$, $\mathbf{u}_0^{(j)} = \mathbf{G}^{(j)}\hat{\mathbf{x}}$ (where $\hat{\mathbf{x}}$ is the estimate of previous iteration of Algorithm 2). Also, the blur kernel estimate (line 4 of Algorithm 2) is computed with 10 iteration of the second instance of Algorithm 3 and initialized with $\mathbf{d}_0^{(j)} = 0$, $\mathbf{u}_0^{(j)} = \mathbf{G}^{(j)}\hat{\mathbf{h}}$ (where $\hat{\mathbf{h}}$ is the estimate of previous iteration of Algorithm 2). The warping parameters of the LR images in the experiments are assumed to be known.

In Figure 2, an applied blur kernel, one LR image, the blur HR image and the best reconstructed HR image are shown for the Cameraman image. The difference in the size of HR image and Blur HR image is due to applying masking matrix $\boldsymbol{M}$.

In Table 1 the structural similarity (SSIM) index [17] of the best reconstructed HR image by the proposed method and the method presented in [16] for all (image, kernel) pairs is illustrated.

The SSIM index ranges from 0 to 1. Its higher value indicates that the reconstructed image is more similar to the original image. As shown in Table 1, the proposed method is superior to the existing method in providing a more quality SR image.

TABLE 1. Comparison between the proposed method (ours) and the method in [16]

Image name	Method	Kernel size		
		7×7	11×11	15×15
Baboon	ours	**0.7093**	**0.5585**	**0.4179**
	[16]	0.6158	0.4534	0.3918
Boat	ours	**0.8814**	**0.7993**	**0.7309**
	[16]	0.8023	0.7110	0.6505
Cameraman	ours	**0.8907**	**0.8381**	**0.7561**
	[16]	0.8190	0.7630	0.7202
Girl	ours	**0.8913**	**0.8359**	0.7793
	[16]	0.8481	0.8343	**0.8004**
House	ours	**0.8707**	**0.8305**	**0.7714**
	[16]	0.8272	0.8114	0.7547
Man	ours	**0.9171**	**0.8433**	**0.7414**
	[16]	0.8178	0.7153	0.6493
Onion	ours	**0.9229**	**0.8725**	**0.7719**
	[16]	0.8517	0.7875	0.6694
Parrot	ours	**0.9272**	**0.8877**	**0.8368**
	[16]	0.8448	0.8127	0.7776
Pepper	ours	**0.8708**	**0.8478**	**0.8012**
	[16]	0.8351	0.8094	0.7912
Tire	ours	**0.9248**	**0.7908**	**0.7104**
	[16]	0.8221	0.7674	0.6295

The reported SSIM of the proposed method is for the best reconstructed HR image

In Another experiment, the proposed method was applied on another fifty natural images. Table 2 shows the average of the SSIM index as well as average of the Mean Square Error (MSE) of all sixty (10 + 50) images for each blur kernel.

Figure 2. (a) Applied blur kernel (11×11), (b) One of LR image, (c) Blur HR image, (d) Reconstructed HR image (SSIM: 0.8381), (e) Result of [16] (SSIM: 0.7630)

TABLE 2. Average of SSIM and MSE of the proposed method (ours) and the method in [16] on 60 test images

Evaluation metric	Method	Kernel size		
		7×7	11×11	15×15
SSIM	ours	**0.9025**	**0.8253**	**0.7296**
	[16]	0.8165	0.7383	0.6690
MSE	ours	**0.0009**	**0.0020**	**0.0037**
	[16]	0.0026	0.0033	0.0045

The reported SSIM of the proposed method is for the best reconstructed HR image.

experiments, the loop in Algorithm 2 is iterated by a predefined number (say, 50 times), then the best reconstructed image is chosen manually. In Figure 3, the SSIM evaluation metric of the reconstructed image in each iteration is shown. Another drawback of the proposed method is that the kernel size must be provided beforehand. In the experiments, the size of the kernel in each dimension is set to the size of the ground truth kernel plus two. As future works, we intend to cope with these deficiencies.
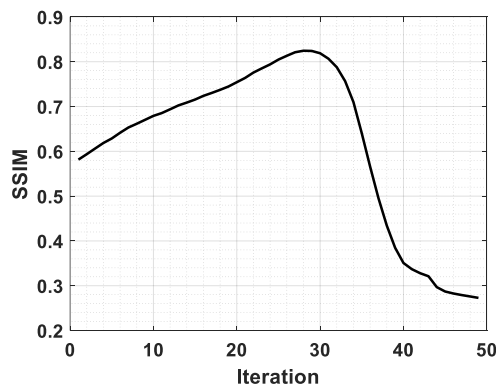
Figure 3. SSIM metric of reconstructed HR image in each iteration

5. CONCLUSIONS

Regularization is a key technique in signal and image reconstruction. In this paper, to reconstruct a high resolution image from some defocus-blurred low resolution images, we propose a new regularizer to apply on unknown blur kernel. The proposed regularizer uses the continuity property of defocus blur kernel. Evaluation results show applying the proposed regularizer improves the quality of the reconstructed high resolution image.

In addition to the mentioned future works in previous section, this research can be extended by finding appropriate regularizer for other types of blur kernel, e.g., Gaussian blur.

6. REFERENCES

1. Babacan, S.D., Molina, R. and Katsaggelos, A.K., "Variational Bayesian super resolution", *IEEE Transactions on Image Processing*, Vol. 20, No. 4, (2010), 984–999.

2. Hassanpour, H. and Seyyedyazdi, S. J., "Improving Super-resolution Techniques via Employing Blurriness Information of the Image", *International Journal of Engineering - Transaction B: Applications*, Vol. 31, No. 2, (2018), 241–249.

3. Almeida, M.S. and Figueiredo, M., "Deconvolving images with unknown boundaries using the alternating direction method of multipliers", *IEEE Transactions on Image Processing*, Vol. 22, No. 8, (2013), 3074–3086.

4. Tsai, R. Y. and Huang, T. ., "Multipleframe image restoration and registration.", *Advances in Computer Vision and Image Processing*, Vol. 1, No. 2, (1984), 317–339.

5. Katsaggelos, A.K., Molina, R. and Mateos, J., "Super resolution of images and video", *Synthesis Lectures on Image, Video, and Multimedia Processing*, Vol. 1, No. 1, (2007), 1–134.

6. Farsiu, S., Robinson, M.D., Elad, M. and Milanfar, P., "Fast and robust multiframe super resolution", *IEEE Transactions on Image Processing*, Vol. 13, No. 10, (2004), 1327–1344.

7. Wang, Z. and Qi, F., "On ambiguities in super-resolution modeling", *IEEE Signal Processing Letters*, Vol. 11, No. 8, (2004), 678–681.

8. Laghrib, A., Ezzaki, M., El Rhabi, M., Hakim, A., Monasse, P. and Raghay, S., "Simultaneous deconvolution and denoising using a second order variational approach applied to image super resolution", *Computer Vision and Image Understanding*, Vol. 168, (2018), 50–63.

9. Fan, J., Wu, Y., Zeng, X., Huangpeng, Q., Liu, Y., Long, X. and Zhou, J., "A Multi-view Super-Resolution Method with Joint-optimization of Image Fusion and Blind Deblurring", *KSII Transactions on Internet and Information Systems (TIIS)*, Vol. 12, No. 5, (2018), 2366–2395.

10. Olshausen, B.A. and Field, D. J., "Emergence of simple-cell receptive field properties by learning a sparse code for natural images", *Nature*, Vol. 381, No. 6583, (1996), 607–609.

11. Levin, A., Fergus, R., Durand, F. and Freeman, W. T., "Image and depth from a conventional camera with a coded aperture", *ACM Transactions on Graphics (TOG)*, Vol. 26, No. 3, (2007), 1–9.

12. Krishnan, D. and Fergus, R., "Fast image deconvolution using hyper-Laplacian priors", In Neural Information Processing Systems Conference, (2009), 1033–1041.

13. Almeida, M.S. and Figueiredo, M. A., "Blind image deblurring with unknown boundaries using the alternating direction method of multipliers.", In 2013 IEEE International Conference on Image Processing, (2013), 586–590.

14. Boyd, S., Parikh, N., Chu, E., Peleato, B. and Eckstein, J., "Distributed optimization and statistical learning via the alternating direction method of multipliers", *Foundations and Trends in Machine Learning*, Vol. 3, No. 1, (2011), 1–122.

15. Boyd, S., Boyd, S.P. and Vandenberghe, L., Convex optimization, Cambridge university press, (2004).

16. Javaran, T.A., Hassanpour, H. and Abolghasemi, V., "Local motion deblurring using an effective image prior based on both the first-and second-order gradients", *Machine Vision and Applications*, Vol. 28, No. 3–4, (2017), 431–444.

17. Wan, Z. and Bovik, A., "Mean squared error: love it or leave it?", *IEEE Signal Processing Magazine*, Vol. 28, No. 1, (2009), 98–117.

Persian Abstract

چکیده

ابرتفکیک‌پذیری فرایندی است که اطلاعات تعدادی تصویرِ با دقت کم از صحنه را ترکیب کرده و تصویری با دقت زیاد از صحنه ایجاد می‌کند. در اغلب کارهای گذشته، فرض می‌شد که تاری اعمال شده به تصاویر کم دقت به خاطر خاصیت انتگرال‌گیری حس‌گر تصویر است. اما در عمل، عامل تاری تصاویر کم دقت می‌تواند به دلایل دیگری باشد، از جمله تاری ناشی از عدم تمرکز عدسی دستگاه اخذ تصویر، تاری ناشی از اغتشاشات جوی و تاری ناشی از حرکت جسم یا دوربین و یا هر دو. در این مقاله فرض بر آن است که کم‌دقتی تصاویر به خاطر عدم تمرکز عدسی تار باشد. بر خلاف تاری ناشی از حرکت که هسته‌ای تُنُک دارد، هسته تاری ناشی از عدم تمرکز عدسی تنک نبوده و یک‌پارچه است. به همین دلیل، ما در این تحقیق گرادیان هسته تاری را با استفاده از منظم‌ساز مناسبی مقید کردیم تا به هسته‌ای یک‌پارچه دست یابیم. نتایج آزمایش‌ها بر روی تصاویر شبیه‌سازی‌شده نشان‌دهنده کارایی روش پیشنهادی برای ایجاد تصویری با دقّت زیاد و رفع تارشدگی با ترکیب تعدادی تصویر کم دقت و تار است.